Check for updates

A quinazolin-based Schiff-base chemosensor for colorimetric detection of Ni²⁺ and Zn²⁺ ions and 'turn-on' fluorometric detection of Zn²⁺ ion†

Vanshika Sharma, Meman Sahu, Amit Kumar Manna, Dinesh De and Goutam Kumar Patra [ID] *

Herein, we have reported a novel quinazolin-based Schiff base chemosensor (*E*)-2-benzamido-*N*′-(1-(pyridin-2-yl)ethylidene)benzohydrazide (**L**). **L** has been designed, synthesised and characterised by ¹H-NMR, IR spectroscopy, ESI-MS spectrometry and theoretical studies. The receptor showed appreciable colorimetric λ_{max} shift for both Ni²⁺ and Zn²⁺ ions and fluorometric "*turn on*" response in presence of only Zn²⁺ ion. The Jobs plot analysis revealed that receptor forms 2 : 1 complex with both the ions Ni²⁺ and Zn²⁺, further confirmed by ESI-MS analysis. The single crystal structure of **L**–Ni²⁺ complex (**1**) has also been determined. The colorimetric detection limits were calculated to 7.9 nM and 7.5 nM respectively for Ni²⁺ and Zn²⁺ in methanol–Tris–HCl buffer medium (10 mM, pH 7.2, 1 : 1 v/v). The chemosensor **L** can be applied for the recovery of contaminated water samples.

Introduction

Metal ion detection continues to be an important area of research both in the environment and in biological systems.[1] Nickel has long been thought of as a potentially toxic metal. Decomposition or degradation of rocks and soil, biological cycles, particularly industrial processes, and water disposal are the main sources of nickel in aquatic systems.[2] The tolerable concentration of Ni(II) ions in drinking water is 2.5 mg mL⁻¹.[3] Among the transition metal series, Ni²⁺ plays a significant part in biological activities like metabolism, respiration, and biosynthesis. It is a necessary component of various metallo-enzymes such hydrogenases, carbon monoxide dehydroge-nases, and acireductone dioxygenases.[4–6] In the chemical industry, it is widely used for the manufacture of practical electronics devices including Ni–Cd batteries, electroplating, and electroforming.[7,8] One of the nickel alloys utilised in the manufacture of tools, machinery, and weapons is stainless steel.[9] The adverse effects of excessive Ni²⁺ accumulation over the recommended limits on human physical health include respiratory issues, lung cancer, pneumonitis, allergies, and central nervous system disorders.[10,11] Thus, one of the difficult issues in current research is the specific detection of Ni²⁺ ion at the biological and environmental level.

Zinc ion is the second-most prevalent heavy metal ion and it is well known that zinc plays a significant role in cellular processes.[12] Because of its structural characteristics, the zinc, a biologically significant metal ion, is essential for many path-ophysiologic processes, including gene expression, cell apoptosis, enzymatic regulation, and neurotransmission.[13–15] The breakdown of Zn²⁺ ion homeostasis, which is toxic in excess or absence may in the pathology of intellectual development as well as other neurological issues including Alzheimer's and Parkinson's diseases.[16,17] Due to this, the detection of Zn²⁺ has been studied intensively. Many selective colorimetric and/or fluorescent probes targeting Zn²⁺ have been reported, that are mostly based on quinoline, fluorescein, benzazole, anthracene, coumarin, BODIPY, Schiff bases, indole, thiazole, terpyridin, naphthalimide, nanoparticles and so on.[18–40]

From the above reports most of them are fluorescent based and few are colorimetric fluorescent chemosensors. Xu *et al.* (2009) has reported an NBD-based colorimetric and fluorescent chemosensor for Zn²⁺ and its use for detection of intracellular zinc ions.[41] S. Lee *et al.* (2016) has reported a Zn²⁺ colorimetric sensor using label-free silver nanoparticles.[42] On the other hand, a fluorescent chemosensor that is "switching on" and selective to Zn²⁺ was described by Li *et al.*[43] and applied in MCF-7 cells. Two new ratiometric chemosensors were also created and tested by Lee *et al.*[44] for the detection of potentially harmful free Zn²⁺ ions in aqueous media. A novel fluorescent chemo-sensor was recently created by Chen and Li *et al.*[45] using a cyclen moiety as the ionophore and a helical imide as the fluorophore. Moreover, Ding *et al.*[46] developed selective and responsive "turn-

Department of Chemistry, Guru Ghasidas Vishwavidyalaya, Bilaspur (C. G.), India. E-mail: patra29in@yahoo.co.in; Tel: +91 7587312992

on" fluorescentric Zn^{2+} sensors based on di- and tri-pyridines with easily modulatable emission wavelengths.

Inspired by the above research and our search on fluorescent colorimetric chemosensor,[47,48] in this work, we have reported an optical sensor for colorimetric detection of Ni^{2+} and Zn^{2+} ions and selective fluorometric detection of Zn^{2+} ion. A quinazolinone derived Schiff base chemosensor (*E*)-2-benzamido-*N'*-(1-(pyridin-2-yl)ethylidene)benzohydrazide (**L**) has been designed, synthesised and characterised by ^{1}H-NMR, IR spectroscopy, ESI-MS spectrometry and single crystal XRD analysis. The receptor showed colorimetric λ_{max} shift for Ni^{2+} and Zn^{2+} (detection limit was 7.9 nM and 7.5 nM respectively) and fluorometric "*turn-on*" response for Zn^{2+} ion with detection limit 1.7 nM in methanol–Tris–HCl buffer medium (10 mM, pH 7.2, 1 : 1 v/v). The Jobs plot analysis revealed that receptor forms 2 : 1 complex with both the ions Ni^{2+} and Zn^{2+}, further confirmed by ESI-MS analysis. The single crystal structure of **L**–Ni^{2+} complex, **3** has also been isolated. The chemosensor **L** can be applied to the recovery of contaminated water samples.

Experimental

Materials and general information

The necessary components were purchased from Sigma-Aldrich and employed for synthesis without further purification. For the majority of the experiments, analytical-grade solvents were utilised, and double-deionized water was used for dilution and the preparation of Tris buffer (pH = 7.2) solution. The metal ion solutions were made from their nitrate salts. ^{1}H-NMR and ^{13}C-NMR spectra were recorded on a Bruker DRX spectrometer operating at 400 MHz in $CDCl_3$ and chemical shifts were recorded in ppm relative to TMS. On a Shimadzu UV 1800 spectrophotometer, absorption spectra were captured using a quartz cuvette with a 10 mm path length and a wavelength of between 200 and 800 nm. Using a Waters mass spectrometer with mixed solvent HPLC methanol and triple-distilled water, high resolution mass (HRMs) spectra were captured. The pH measurements were done using a digital pH meter (Merck) by adjusting dilute hydrochloric acid and sodium hydroxide in buffer solution. Solutions of the receptor **L** (1×10^{-5} M) and metal salts (1×10^{-4} M) were prepared in CH_3OH–H_2O (1 : 1, v/v) and H_2O respectively.

X-ray data collection and structural determination

X-ray single crystal data were collected using MoKα ($\lambda = 0.7107$ Å) radiation on a BRUKER APEX II diffractometer equipped with CCD area detector. Data collection, data reduction, structure solution/refinement were carried out using the software package of SMART APEX.[49] The structures were solved by direct methods (SHELXS-97) and standard Fourier techniques, and refined on F^2 using full matrix least squares procedures (SHELXL-97) using the SHELX-97 package[50] incorporated in WinGX.[51] In most of the cases, non-hydrogen atoms were treated anisotropically. Hydrogen atoms were fixed geometrically at their calculated positions following riding atom model. Structural information of **3** have been deposited at the Cambridge Crystallographic Data Center (CCDC number 2205292†).

Synthesis of 2-phenyl-4(3*H*)-3,1-benzoxazinone (1)

The 2-phenyl-4*H*-benzoxalin-4-one (**1**) has been synthesized by following the reported procedure[52] with some modification. To a stirred solution of anthranilic acid (2.74 g, 0.020 mol) in pyridine (12 mL), benzoyl chloride (2.81 g, 0.020 mol) was added dropwise, maintaining the temperature about 0–5 °C for 1 h. The reaction mixture was stirred for another 3 h at room temperature until a solid product was formed. The reaction mixture was neutralized with saturated sodium bicarbonate solution and the pale yellow solid which separated was filtered, washed with water and re-crystallized from ethanol. Yield, 3.8 g, 85%; mp 112–115 °C. ^{13}C NMR (400 MHz, $CDCl_3$, TMS): δ 100.2 (1C, C=N), 130.4–137.0 (12C, aromatic carbons), 172.1 (1C, C=O). ^{1}H NMR (400 MHz, $CDCl_3$, TMS): δ 8.31 (d, 2H), 8.24 (d, 1H), 7.82 (t, 1H), 7.69 (d, 1H), 7.58 (t, 1H), 7.51 (m, 3H) (Fig. S1†).

Synthesis of 3-amino-2-phenyl-4(3*H*)-quinazolinone (2)

To a stirred solution of **1** (2.23 g, 0.01 mol) in ethanol (20 mL), 80% $N_2H_4 \cdot H_2O$ (0.5 g, 0.01 mol) and a catalytic amount of pyridine (2–4 drop) was added. The reaction mixture was stirred and refluxed for 2 h at 117 °C. After cooling, the crude product was obtained by filtration and the crude product was recrystallized from ethanol to afford **2** as a white product.[53] Yield, 2.15 g, 90%; mp 178–180 °C. ^{13}C NMR (400 MHz, $CDCl_3$, TMS): δ 110.5 (1C, C=N), 126.6–140.3 (12C, aromatic carbons), 167.4 (1C, C=O). ^{1}H NMR (400 MHz, $CDCl_3$, TMS): δ 8.45 (d, 2H), 7.92 (s, 1H), 7.68 (m, 4H), 7.51 (d, 2H), 6.85 (s, 2H) (Fig. S2†).

Synthesis of *N*-(*E*)-*N'*-(4-(diethylamino)-2-hydroxybenzylidene)-2-(benzamido) benzohydrazide (L)

2.37 g (0.01 mol) of **2** was dissolved in 20 mL of absolute ethanol and to this solution 1.21 g (0.01 mol) 1-(pyridin-2-yl)ethanone was added dropwise with constant stirring. Then the reaction mixture was refluxed for 12 h under dry condition. The resulting mixture was kept in air for 24 h. Needle shaped crystals separated out was filtered, washed with methanol and dried in air. Yield, 3.15 g, 87%; mp = 235–237 °C. Single crystals suitable for X-ray analysis were obtained from the slow evaporation of dichloromethane solution of **L**. Anal. calc. for $C_{21}H_{18}N_4O_2$: C, 70.38; H, 5.06; N, 15.63. Found C, 70.68; H, 5.05; N, 15.07%. EI-MS: *m/z* 359.14 (M + Na^+, 100%); (Fig. S3†). FTIR/cm^{-1} (KBr): 3216 (-NH), 3040 (m, aromatic CH– str), 1676 (*vs.*, C=O), 1631 (*vs.*, C=N), 1525 (s), 1454 (s), 1370 (m), 1316 (s), 1260 (s), 1167 (s), 1092 (s), 1037 (m), 972 (s), 934 (s) (S4). ^{1}H NMR (400 MHz, $CDCl_3$, TMS): δ 11.57 (s, NH), 11.32 (s, 1H, NH), 8.87 (s, 1H, azomethine), 8.1–6.9 (m, 12H, aromatic), 1.19 (s, 3H, methyl) (Fig. S5†). ^{13}C NMR ($CDCl_3$, δ ppm, TMS): 165.81, 158.93, 151.27, 139.01, 134.09, 132.67, 131.31, 130.38, 129.39, 129.22, 128.35, 128.09, 127.61, 127.02, 126.76, 123.63, 122.34, 119.60, 117.72, 117.52, 19.45 (Fig. S6†).

Synthesis of Ni^{2+} complex of L (NiL_2, 3)

A methanolic solution (10 mL) of $Ni(NO_3)_2 \cdot 3H_2O$ (0.120 g, 0.5 mmol) was added dropwise with stirring to the saturated

solution of **L** (0.181 g, 0.5 mmol) in methanol (20 mL). The resulting mixture was continuously stirred for 1 h at room temperature and then filtered. Yield, 69%. Anal. calc. for $C_{42}H_{36}N_8NiO_4$: C, 65.05; H, 4.68; N, 14.45%. Found C, 64.96; H, 4.59; N, 14.53%. EI-MS: m/z 772.2 ($2L-2H^+ + Ni^{2+}$) (Fig. S7†). FTIR/cm^{-1} (KBr):3440 (–NH), 3024 (m, aromatic CH– str), 1660 ($vs.$, C=O), 1606 ($vs.$, C=N), 1504 (s), 1443 (m), 1385 (s), 1313 (s), 1216 (s), 1167 (s), 1037 (m), 708 (s) (Fig. S8†). Slow evaporation of the methanol solution of **3** yielded dark red crystalline solid (suitable for X-ray analysis).

Synthesis of Zn^{2+} complex of L (ZnL$_2$, 4)

A methanolic solution (10 mL) of $Zn(NO_3)_2 \cdot 6H_2O$ (0.150 g, 0.5 mmol) was added dropwise with stirring to the saturated solution of **L** (0.181 g, 0.5 mmol) in methanol (20 mL). The resulting mixture was continuously stirred for 1 h at room temperature and then filtered. Yield, 72%. Anal. calc. for $C_{42}H_{36}N_8ZnO_4$: C, 64.49; H, 4.64; N, 14.33%. Found C, 64.56; H, 4.55; N, 14.47%. EI-MS: m/z 803.2 ($2L + Zn^{2+} + Na^+$) (Fig. S9†). FTIR/cm^{-1} (KBr): 3068 (w), 2928 (m), 1665 ($vs.$, C=O), 1643 ($vs.$, C=N), 1595 (s), 1519 (s), 1446 (m), 1342 (m), 1242 (s), 1137 (m), 762 (m), (Fig. S10†).

Photo physical measurements

Chemosensor **L** (3.58 mg) was dissolved separately in 10 mL of homogeneous solvent $CH_3OH–H_2O$ (1 : 1, v/v) to make a solution of 1×10^{-3} M and 30 μL of each of this solution were diluted with 2.97 mL of CH_3OH–Tris buffer (1 : 1 v/v) mixture to make a final concentration of 10 μM. The analyte solutions have been prepared using nitrate salt of metals in the order of 10^{-4} M in double-distilled water. After mixing **L** with each of the metal ions for a few seconds, absorption and fluorescence spectra were obtained at room temperature.

Job's plot measurements

A methanol–Tris buffer (1 : 1) solutions containing **L** (10 μM) and aqueous solution of $Ni(NO_3)_2$ and $Zn(NO_3)_2$ (10 μM each) were prepared separately. Then changing the mole ratio of the **L** from 0.1 to 0.9 in such a manner that the sum of the total metal ion and **L** volume remained constant (2 mL). All the solutions were diluted to 3 mL. After shaking them for a minute, UV-vis spectra were obtained at room temperature.

Computational details

The program package GAUSSIAN-09 Revision C.01 was employed for all calculations.[54] The gas phase geometries of the compound were fully optimized symmetry restrictions in singlet ground state with the gradient-corrected DFT level coupled with B3LYP.[55] Basis set LanL2DZ was used for the whole molecules **L** and NiL$_2$ (**3**). The HOMOs and LUMOs of molecular ions were calculated with the same basis set and functional.
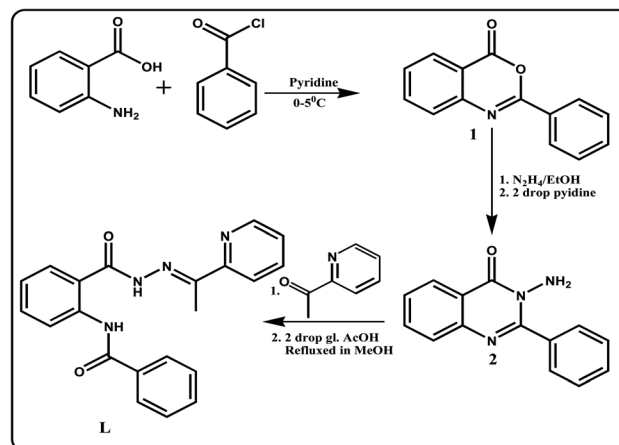
Scheme 1 Synthesis procedure of ligand **L**.

Result and discussion

Synthesis and structure of L

The coupling reaction between aldehyde and amine generate the imine functionalised ligand **L** (Scheme 1) with high yield (over 85%) and it was characterised by elemental analysis, FTIR, ^{1}H NMR and ESI-mass spectra.

UV-vis spectroscopic studies of L towards different metal ions

The receptor contains imine linker as well as several amide functional moieties thus interaction with cations and anions were expected. Thus absorption studies of **L** in presence of common cations and anions were performed at room temperature in methanol–Tris–HCl buffer (1 : 1 v/v, 10 mM, pH 7.2) solution. The receptor **L** shows main absorption band at 280 nm due to π–π* transition. This absorption band of **L** significantly red shifted to around 375 nm only in presence of 2 equiv. of Ni^{2+} and Zn^{2+} ions with the change of colour of the solution from colourless to yellow. Addition of same amount of several metal like Cu^{2+}, Co^{2+}, Cd^{2+}, Cr^{3+}, Mn^{7+}, Sm^{3+}, Al^{3+} to the solution of receptor **L**, also absorption band shift observed, but the color and absorbance intensity produced by these ions is not very prominent when compare with Ni^{2+} and Zn^{2+} ions. The remaining cations and anions $e.g.$ Fe^{3+}, Hg^{2+}, Pb^{2+}, Cr^{3+}, Ag$^+$, Mn^{2+}, Fe^{2+} $etc.$ cannot produced any significant change of receptor solution at that condition (Fig. S11†).

After that, using same UV-vis spectrophotometer, receptor **L** was titrated separately in presence of Ni^{2+} and Zn^{2+} ions in methanol–Tris–HCl buffer (1 : 1 v/v, 10 mM, pH 7.2) solution. Here successive amount addition of analyte ions to the ligand **L**, absorption band gradually enhanced at ~375 nm for Ni^{2+} whereas 333 nm and 375 nm for Zn^{2+} ion. As a results the absorption band at 280 nm goes on decreasing simultaneously and well-defined isosbestic point developed at 332 nm and 331 nm for Ni^{2+} and Zn^{2+} ions respectively. This change in absorption behaviour of **L** with addition of Ni^{2+} and Zn^{2+} ions remained consistent up to 0.5 equiv. for both ions and then remained well saturated (Fig. 1).
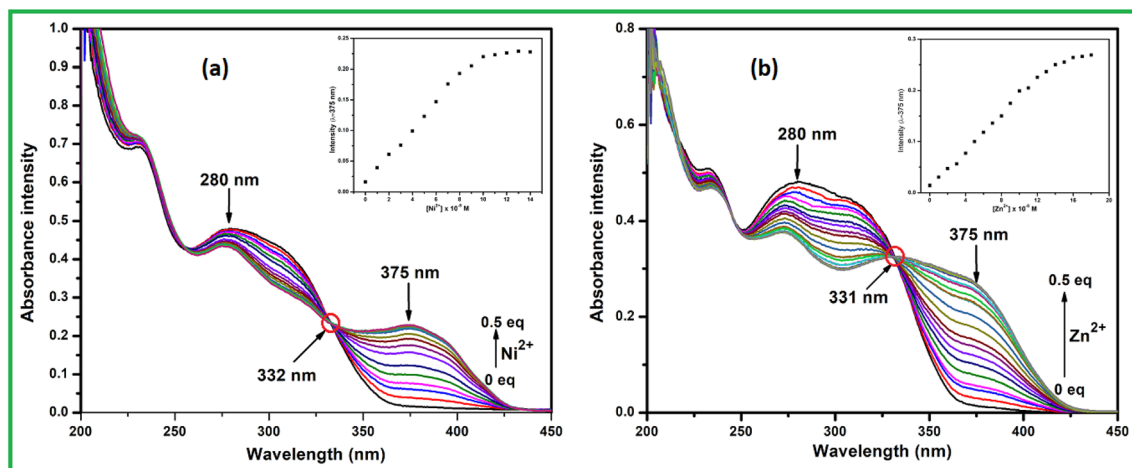
Fig. 1 UV-vis titration of **L** with (a) Ni^{2+} and (b) Zn^{2+} in methanol–Tris–HCl buffer. (Inset) Plot of intensity *vs.* analyte concentration.
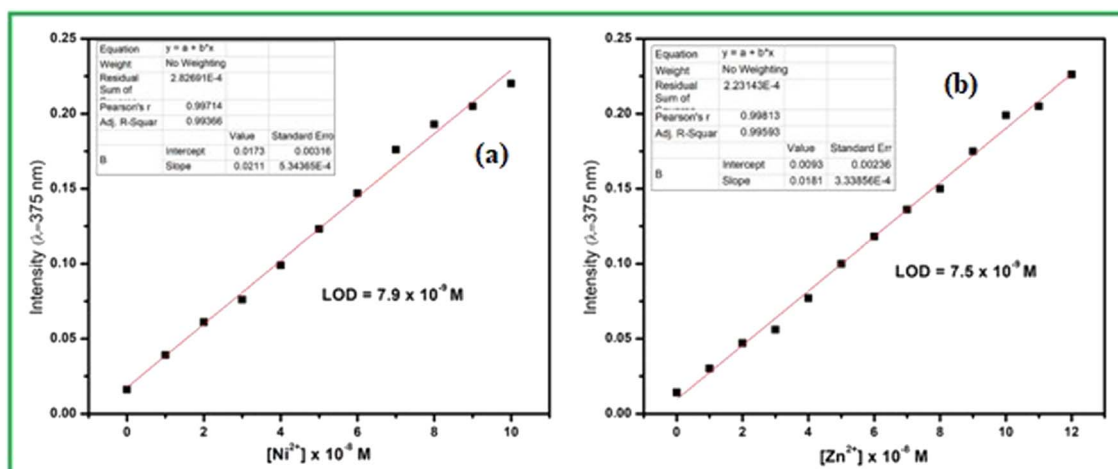

Fig. 2 Colorimetric detection limit of (a) Ni^{2+} (b) Zn^{2+}.

From the titration experiments the calibration curves were plotted where the absorbance intensity around 375 nm for both the metal ions varies almost linearly with the concentration. Thus detection limit was calculated to 7.9×10^{-9} M for Ni^{2+} and 7.9×10^{-9} M for Zn^{2+} using convenient formula DL = $3\sigma/m$, here 'σ' is standard deviation of the blank measurement and 'm' is the slope of the linear calibration curve (Fig. 2). This low level DL values are far below the guideline provided by WHO in drinking water and several reported Ni^{2+} and Zn^{2+} sensors. As per WHO, the permissible limits of Ni^{2+} and Zn^{2+} ions in drinking waters are 0.0008 and 5.0 mg L^{-1} respectively.[56]

The precise detection of analyte like Zn^{2+} and Ni^{2+} ion in real water sample can be hampered in presence of other interfering ions due to their cross responses. Thus analyte signalling of receptor **L** was performed in presence of common competing ions as a background. The presence of same equivalent of other interfering cations with analyte ion, the absorption spectra of host–guest complex cannot be disturbed (Fig. 3). Even 3 fold excessive addition of competitive metal ions than analyte, the
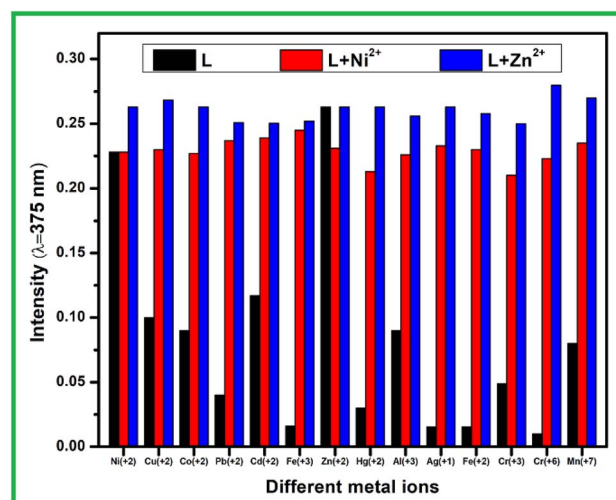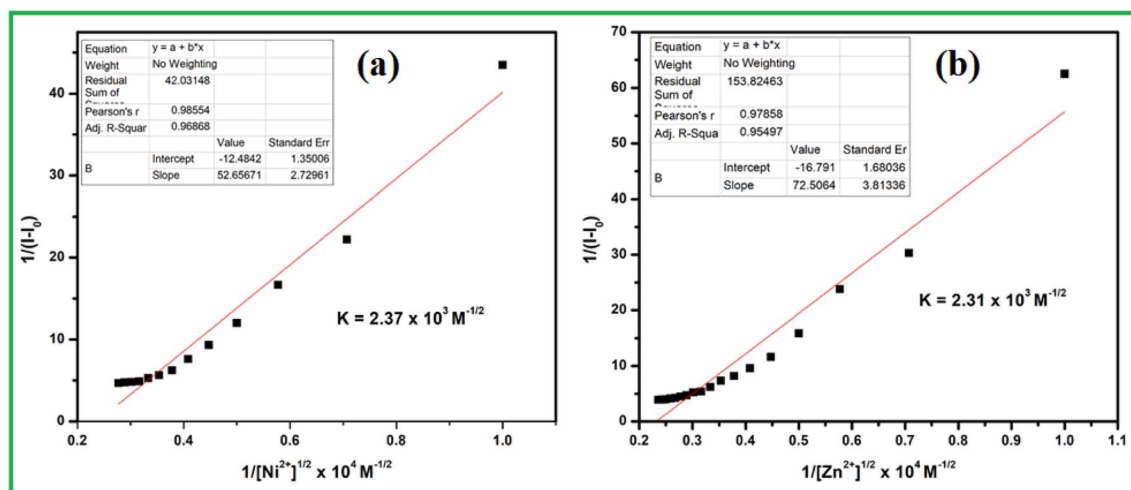

Fig. 3 Interference test of **L** with different metal ions.

Fig. 4 Association constant for (a) Ni^{2+} (b) Zn^{2+}.

original peak intensity of $L + M^{2+}$ remained almost negligible change. Moreover, presence of equal amount of Zn^{2+} ion to the $L–Ni^{2+}$ solution can replace Ni^{2+}, thus corresponding absorbance band intensity to $L–Zn^{2+}$ complex was observed.

The Job's plot indicates that here 2 : 1 binding stoichiometric ratio obtained between receptor **L** and both the analyte metal ions Ni^{2+} and Zn^{2+} (Fig. S12†), which was further confirmed by ESI-MS analysis (Fig. S7 and S9†) and single crystal structure of the $L–Ni^{2+}$ (3) was isolated complex (*vide infra*). In the ESI-MS spectra peaks at m/z 772.2 (Fig. S7†) and m/z at m/z 803.2 (Fig. S9†) indicated 2 : 1 binding stoichiometric ratio between the ligand **L** and the metal ions Ni^{2+} and Zn^{2+} respectively. Assuming 2 : 1 host–guest ratio, the association constants were calculated from Benesi–Hildebrand (B–H) equation by the linear fitting of graph $1/(A - A_0)$ *vs.* $1/[M^{2+}]^{1/2}$ (Fig. 4). The values obtained as $2.37 \times 10^3 \ M^{-1/2}$ and $2.31 \times 10^3 \ M^{-1/2}$ for Ni^{2+} and Zn^{2+} ion respectively, indicates very strong affinity between receptor and analytes.

As we are interested on analyte sensing in aqueous or semi aqueous medium, thus pH of this medium plays a very crucial

Fig. 5 pH effect test.

role as receptor contain pH sensitive amide (–CONH–) and imine (>C=N) moieties. For that purpose, receptor solutions with variable pH range 2 to 12 were adjusted by dilute HCl and NaOH and then analyte ions were added independently. The sequential UV-vis studies of each set of solution indicates that absorbance intensity at 375 nm for **L** and its metal complexes are mostly increases with pH. At pH = 2–4, there is less absorbance intensity difference observed between **L** and $L + M^{2+}$ (M = Zn and Ni), thus not very suitable to sense at this pH range. Thus in a wide range of pH = 5–12 the proposed chemosensor can successfully sense both Ni^{2+} and Zn^{2+} ion including physiological environment (Fig. 5).

Generally, metal ions like Ni^{2+} and Zn^{2+} ion form stable chelate complex with multidentate ligand Na_2EDTA. Thus reversibility was checked by absorption studies $L + M^{2+}$ (M = Zn and Ni) solution with Na_2EDTA in working medium. The characteristic absorption bands of host–guest complexes around 375 nm, instantly disappeared when $L + M^{2+}$ (M = Zn and Ni) complex reacted with 1 equiv. Na_2EDTA (Fig. 6). Thus absorbance intensity at 280 nm restored with solution turns yellow to colourless due to generation of **L**. Further addition of analytes, the absorbance intensity at 375 nm was almost recovered. The alternative addition of chelator and analytes, absorption switching between **L** and $L + M^{2+}$ were almost consistent up to 4 cycles with negligible loss of absorbance intensity which indicate that sensing process is reversible than any irreversible metal catalysed reaction.

Fluorescence studies

The emission properties of the receptor **L** in presence of selective metal ions was also examined in methanol–Tris–HCl buffer (10 mM, pH 7.2) mixture (1 : 1 v/v). Among the selected metal ions like Fe^{3+}, Cu^{2+}, Co^{2+}, Ni^{2+}, Zn^{2+}, Cd^{2+}, Hg^{2+}, Pb^{2+}, Cr^{3+}, Ag^+, Al^{3+}, Mn^{2+} and Fe^{2+} only addition of 2 equiv. Zn^{2+} ion to the ligand solution emission intensity at 463 nm significantly enhanced whereas the same amount of other metal ions including Ni^{2+} induced very significant emission change of receptor **L** (Fig. 7). To
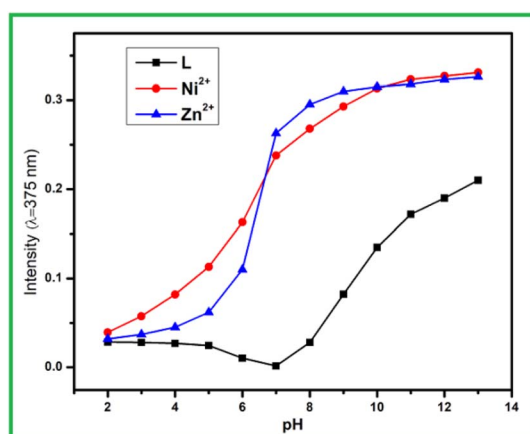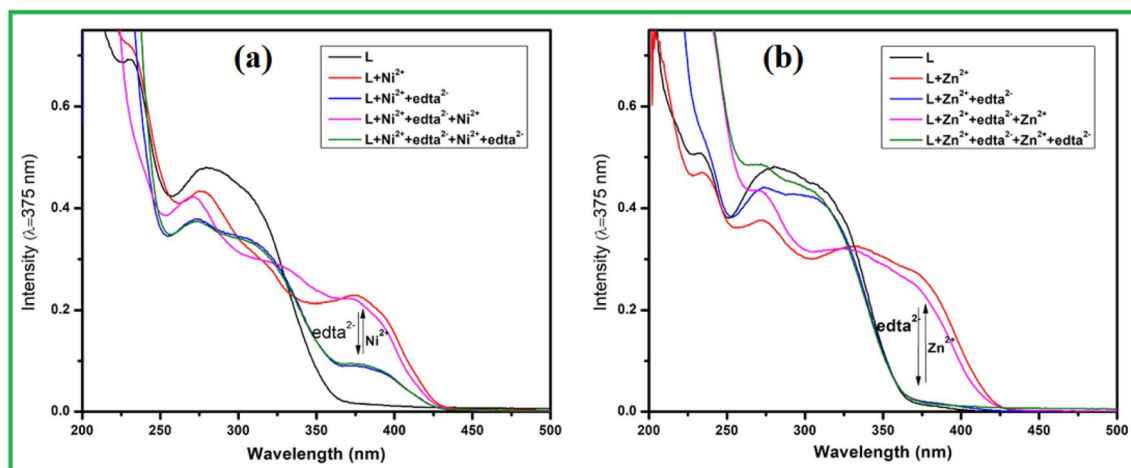
Fig. 6 Absorbance spectra of L in the absence and presence of (a) Ni^{2+} and Na_2EDTA, and (b) Zn^{2+} and Na_2EDTA.
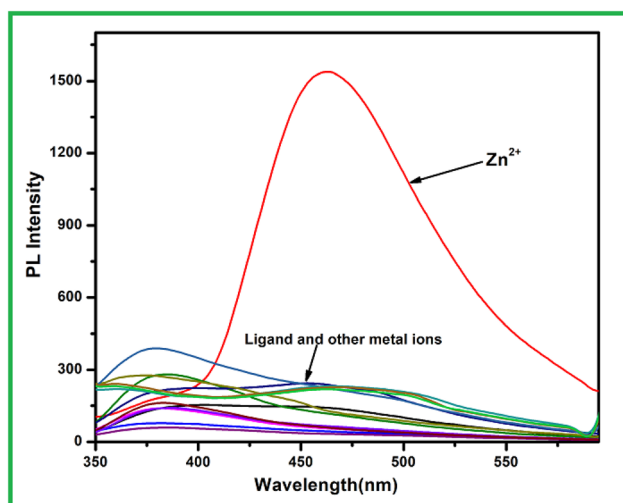

Fig. 7 Fluorescence selectivity of the receptor L in methanol–Tris–HCl buffer.

get the details aspect of the emission spectra, titration experiment was conducted. When excited at 290 nm free receptor L showed weak emission at 455 nm. Upon increasing the Zn^{2+} ion concentration in the receptor solution, emission intensity gradually enhanced with slightly red shifted to 463 nm that got saturated up to 5 equiv. of Zn^{2+} ion (Fig. 8a). The metal ion coordination with receptor L *via* imine side probably restricted both the non-radiative PET and $>C=N$ isomerisation process, thus emission intensity increase due to chelation enhancement fluorescence effect (CHEF). At the same time, there is no change in emission intensity of L in case of Ni^{2+} ion indicate that in L–Ni^{2+} complex both the opposing process *i.e.* paramagnetic fluorescence quenching and chelation enhancement fluorescence effect mutually compensate to each other. The emission enhancement of L in presence of Zn^{2+} ion, cannot be disturbed in addition of 2-fold higher concentration of other metal ions. The fluorometric detection limit was found to 1.7×10^{-9} M calculated using the same formula $3\sigma/m$ (Fig. 8b).
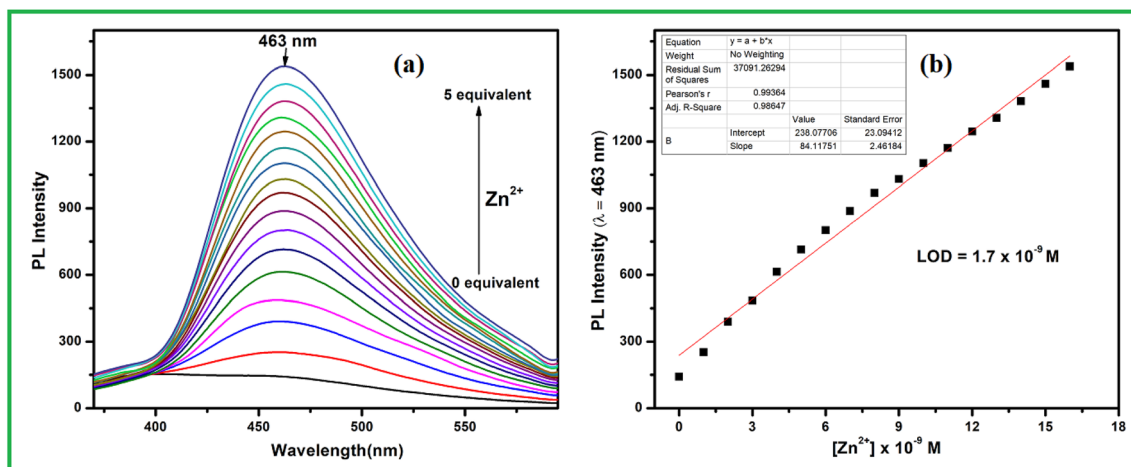

Fig. 8 (a) Fluorescence titration of L with Zn^{2+} (b) fluorometric limit of detection for Zn^{2+}.

DFT calculation

The geometry optimizations staring from the Gauss-view structure of **L** lead to a global minimum as a stationary level. The optimized structures of the **L** and its Ni^{2+} complex (**3**) and schematic representation of the energy of MOs and contours of selected HOMO and LUMO orbitals of **L** and **3** are presented in Fig. 9. The HOMO to LUMO energy gap for **L** is 3.25 eV, whereas for **3**, the gap is 2.92 eV.

X-ray single crystal structure of NiL_2 (3)

The ligand **L** reacts with $Ni(NO_3)_2$ (2 : 1 molar ratio) in methanol at room temperature to form the complex **3**. It crystallizes in the monoclinic space group $C2/c$ (Table 1). The asymmetric unit consists of one **L** ligand and one Ni^{2+} ion (Fig. 10a) with occupancy half. The overall complex contains one Ni^{2+} ion and two **L** ligands (Fig. 10b). The metal ion shows distorted octahedral coordination with N_4O_2 donor sets from
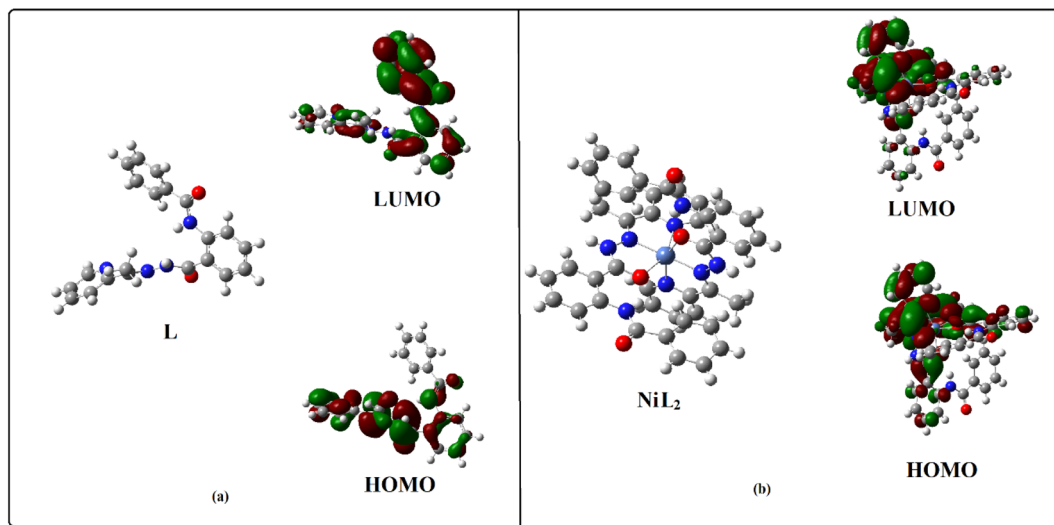

Fig. 9 (a) Energy minimized structure of the **L** and NiL_2 (**3**); (b) a schematic representation of the energy of MOs and contours of selected HOMO and LUMO orbitals of **L** and NiL_2.

Table 1 Crystal data and structure refinement for **3**

| Empirical formula	$C_{42}H_{34}N_8NiO_4$
Formula weight	773.48
Temperature/K	221.68
Crystal system	Monoclinic
Space group	$C2/c$
$a/\text{Å}$	24.902(7)
$b/\text{Å}$	11.539(3)
$c/\text{Å}$	16.250(6)
$\alpha/°$	90
$\beta/°$	127.330(17)
$\gamma/°$	90
Volume/Å^3	3713(2)
Z	4
ρ_{calc} g cm^{-3}	1.384
μ/mm^{-1}	0.578
$F(000)$	1608.0
Crystal size/mm^3	$0.25 \times 0.22 \times 0.18$
Radiation	$MoK\alpha$ ($\lambda = 0.71073$)
2θ range for data collection/°	5.022 to 50.208
Index ranges	$-29 \leq h \leq 29, -13 \leq k \leq 13, -19 \leq l \leq 19$
Reflections collected	17 858
Independent reflections	2761 [$R_{int} = 0.2075, R_{sigma} = 0.1661$]
Data/restraints/parameters	2761/0/250
Goodness-of-fit on F^2	1.073
Final R indexes [$I \geqq 2\sigma (I)$]	$R_1 = 0.0978$, w$R_2 = 0.1692$
Final R indexes [all data]	$R_1 = 0.1542$, w$R_2 = 0.1924$
Largest diff. peak/hole/e Å^{-3}	0.43/-1.11
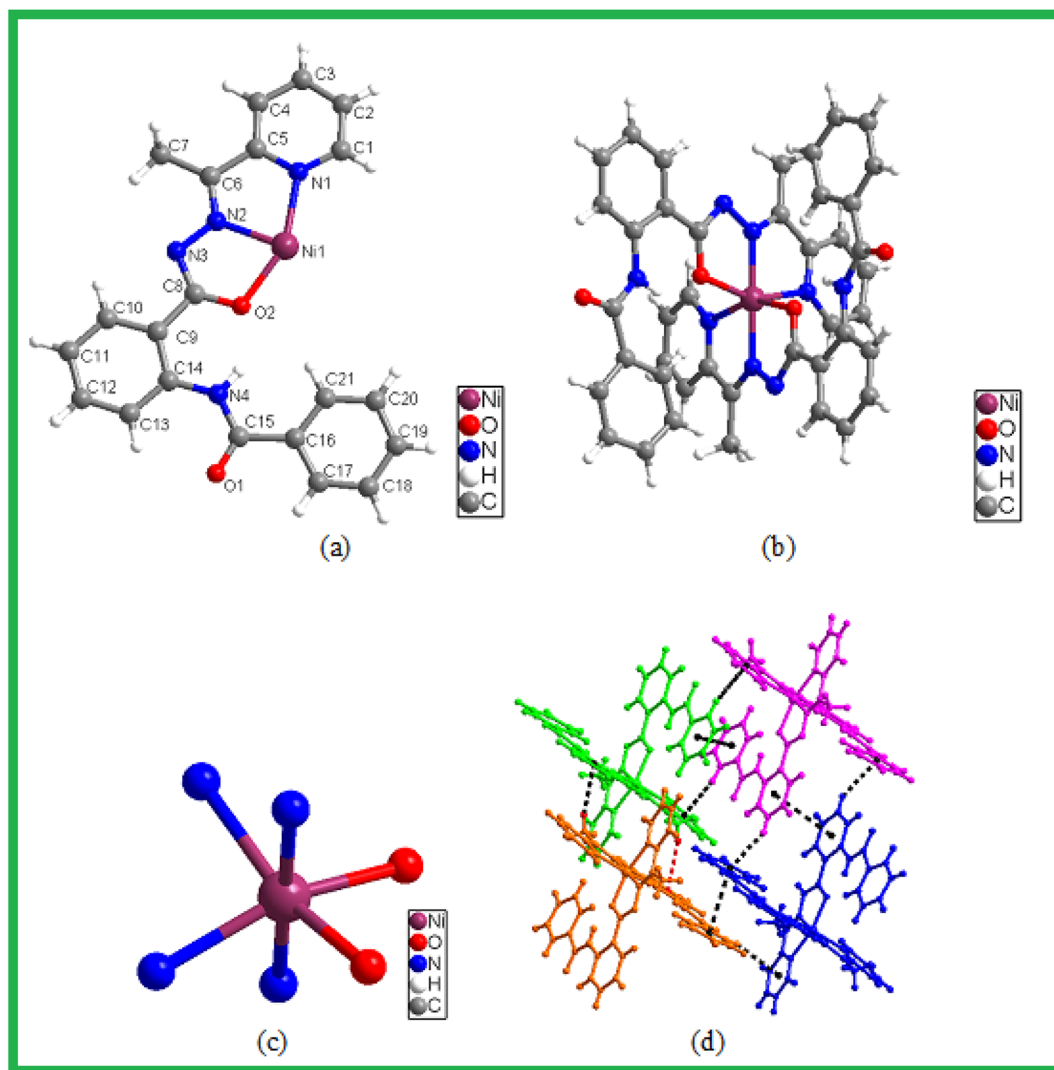
Fig. 10 (a) Asymmetric unit of 3, (b) overall structure of the complex 3, (c) coordination environment around the Ni^{2+} ion, (d) view of 3 illustrating the intramolecular π–π stacking and CH–π interactions (dotted line).

two pyridyl N, two amide O and two hydrazide N (Fig. 10c). The Ni–N and Ni–O bond distances and bond angles (Tables S1 and S2†) were found to be within normal ranges. The charges on Ni(II) ion were internally compensated by two deprotonated hydrazide NH originating from two L. Carefully looking into the structure of 1 revealed that the complex is associated through intermolecular π–π stacking and CH–π interactions (Fig. 10d).

Comparison of the performance of L with other reported fluorescent and colorimetric chemosensors

Colorimetric detection of Ni^{2+} and Zn^{2+} ions and 'turn-on' fluorometric detection of Zn^{2+} ion using a single probe is not very common in the literature. Compared to the other systems, our system has several attractive analytical features, such as high sensitivity, wide linear range, high selectivity, lower

detection limit, simple operation technology, good solubility, sensitive visualization and good practical applicability (Table 2). Moreover, the synthesis of our proposed chemosensor L requires only two steps and less hazardous reagents, and no hazardous by-product is formed.

Application

To explore the Ni^{2+} and Zn^{2+} sensing ability of the present chemosensor L in real water samples, we have tested the probe L in waste water and we got some result. Artificial M^{2+} (M = Ni, Zn) polluted tap water samples have been made by adding known amounts of standard M^{2+} solutions in order to test its sensing in various samples. The prepared samples were analyzed by the same UV-vis spectrometer and the recovery amounts were calculated using the calibration curve (intensity vs. conc.) with the help of Lambert–Beer law. As shown in Table 3, the M^{2+} concentration recovered for each sample are close in agreement with spiked

Table 2 Comparison of the performance of **L** with other reported chemosensors

| Type of sensors | Ion sensing | Limit of detection (M) | | Reference |
		Colorimetrically	Fluorometrically	
Aminopyridine Schiff bases based	Ni^{2+}, Zn^{2+}	6.96×10^{-7} and 4.17×10^{-7}	—	57
	Zn^{2+}	—	1.13×10^{-7}, 2.95×10^{-7}	57
Aminoantipyrine based	Zn^{2+}	—	1.4×10^{-8}	58
Octopamine-based	Zn^{2+}	—	9.9×10^{-7}	59
Benzothiazole-based	Ni^{2+}, Zn^{2+}	Not provided	2.50×10^{-7} and 3.0×10^{-7}	60
Naphthalimide-based	Ni^{2+}, Zn^{2+}	—	3.3×10^{-7} and 1.8×10^{-7}	61
Quinazolin-based	Ni^{2+}, Zn^{2+}	7.9×10^{-9} and 7.5×10^{-9}	—	This work
	Zn^{2+}	—	1.7×10^{-9} M	This work

Table 3 Analysis of M^{2+} (nM) in water sample by the developed method (mean ± standard deviation, $n = 3$)

Sample	M^{2+} added	M^{2+} found	Recovery (%)	Relative error (%)
Ni^{2+}	5	5.02 ± 1.5	100.5	0.4
	10	10.15 ± 1.54	101.5	1.5
	20	19.70 ± 0.87	98.5	2.0
Zn^{2+}	5	5.13 ± 0.97	102.6	2.6
	10	9.87 ± 1.1	98.7	1.3
	20	20.06 ± 1.2	100.3	0.6

amount with good precision. Thus, the receptor **L** can be suitable to detect M^{2+} ion quantitatively in real water samples, indicating that it could be applied in real environments (Table 3).

Conclusion

In summary, we have successfully designed and synthesized a quinazolinone derived Schiff base chemosensor **L** for colorimetric nanomolar detection of Ni^{2+} and colorimetric fluorescent detection of Zn^{2+} with high selectivity and sensitivity over other competitive ions in aqueous medium. A 2 : 1 stoichiometry between **L** and Ni^{2+} were supported by Job-plot, ESI-mass spectral analysis and DFT studies. The single crystal of the **L** + Ni^{2+} was also isolated. The colorimetric detection limits reached up to 7.9 nM for Ni^{2+} and 7.5 nM for Zn^{2+} respectively. Fluorescent measurement of Zn^{2+} were obtained with the detection limit of 1.70 nM, which were far lower than those recommended by the WHO guidelines for drinking water. The reversible response to Ni^{2+} and Zn^{2+} ion was established by the Na_2EDTA experiments. Moreover, **L** could operate in a wide range of pH and can be successfully applied for detection and quantification of Ni^{2+} in environmental samples.

Conflicts of interest

Authors declare no conflicts of interest.

Acknowledgements

References

1 P. de Silva, H. Q. N. Gunaratne, T. Gunnlaugsson, A. J. M. Huxley, C. P. McCoy, J. T. Rademacher and T. E. Rice, *Chem. Rev.*, 1997, **97**, 1515.

2 *Elements and their compounds in the environment*, ed. E. Merian, M. Anke, M. Ihnat and M. Stoeppler, Wiley-VCH, Weinheim, 2nd edn, 2004, pp. 1113–1124.

3 H. L. Bohn, B. L. McNeal, and G. A. O'Connor, *Soil Chemistry*, Wiley Interscience, Chichester, UK, 2nd edn, 1985.

4 B. Zambelli, F. Musiani, S. Benini and S. Ciurli, *Acc. Chem. Res.*, 2011, **44**, 520.

5 S. W. Ragsdale, *J. Biol. Chem.*, 2009, **284**, 18571.

6 R. J. Maier, *Biochem. Soc. Trans.*, 2005, **33**, 83.

7 K. S. Kasprzak, F. W. Sunderman and K. Salnikowa, *Mutat. Res.*, 2003, **533**, 67.

8 P. H. Kuck, *Mineral Commodity Summaries: Nickel*, United States Geological Survey, 2006.

9 J. R. Davis, *Nickel, cobalt, and their alloys*, ASM International, 2000, vol. 7.

10 W. Lee, K. A. Davis, R. L. Rettmer and R. F. Labbe, *Am. J. Clin. Nutr.*, 1988, **48**, 286.

11 X. Q. Liu, X. Zhou, X. Shu and J. Zhu, *Macromolecules*, 2009, **42**, 7634.

12 J. M. Berg and Y. Shi, *Science*, 1996, **271**, 1081.

13 K. H. Falchuk, *Mol. Cell. Biochem.*, 1998, **188**, 41–48.

14 W. Maret, C. Jacob, B. L. Vallee and E. H. Fischer, *Proc. Natl. Acad. Sci. U. S. A.*, 1999, **96**, 1936–1940.

15 H. H. Sandstead, *J. Trace Elem. Exp. Med.*, 2003, **16**(4), 165–173.

16 J. A. Duce, A. Tsatsanis, M. A. Cater, *et al.*, *Cell*, 2010, **142**, 857–867.

17 E. M. Alvarez, R. S. Otero, A. H. Ameijeiras, A. M. L. Real and J. L. L. Garcia, *Biochim. Biophys. Acta*, 2002, **1586**, 155–168.

18 T. Liu and S. Liu, *Anal. Chem.*, 2011, **83**, 2775–2785.

19 D. Dong, X. Jing, X. Zhang, X. Hu, Y. Wu and C. Duan, *Tetrahedron*, 2012, **68**, 306–310.

20 A. Helal, M. Harun, M. Rashid, C. H. Choi and H. S. Kim, *Tetrahedron*, 2012, **68**, 647–653.

21 P. Ashokkumar, V. T. Ramakrishnan and P. Ramamurthy, *J. Phys. Chem. A*, 2011, **115**, 14292–14299.

22 Z. Xu, J. Yoon and D. R. Spring, *Chem. Soc. Rev.*, 2010, **39**(6), 1996–2006.

23 L. Xue, C. Liu and H. Jiang, *Chem. Commun.*, 2009, **9**, 1061–1063.

24 Y. Liu, N. Zhang, Y. Chen and L. H. Wang, *Org. Lett.*, 2007, **9**, 315–318.

25 H. A. Michaels, C. S. Murphy, R. J. Clark, M. W. Davidson and L. Zhu, *Inorg. Chem.*, 2010, **49**, 4278–4287.

26 H. K. Jin, Y. N. Jin, I. H. Hwang, J. Kang, J. Kim and C. Kim, *Tetrahedron Lett.*, 2013, **54**, 2415–2418.

27 D. Maity and T. Govindaraju, *Chem. Commun.*, 2012, **48**, 1039–1041.

28 J. Li, C. F. Zhang, Z. Z. Ming, G. F. Hao, W. C. Yang and G. F. Yang, *Tetrahedron*, 2013, **69**, 4743–4748.

29 N. Boens, V. Leen and W. Dehaen, *Chem. Soc. Rev.*, 2012, **41**, 1130.

30 A. N. Kursunlu, E. Guler, H. I. Ucan and R. W. Boyle, *Dyes Pigm.*, 2012, **94**, 496–502.

31 G. Consiglio, S. Failla, I. P. Oliveri, R. Purrello and B. S. Di, *Dalton Trans.*, 2009, **47**, 10426–10428.

32 Y. Zhou, Z. X. Li, S. Q. Zang, Y. Y. Zhu, H. Y. Zhang, H. W. Hou and T. C. Mak, *Org. Lett.*, 2012, **14**, 1214.

33 K. Hanaoka, K. Kikuchi, H. Kojima, Y. Urano and T. Nagano, *J. Am. Chem. Soc.*, 2004, **126**, 12470–12476.

34 A. Ding, F. Tang, T. Wang, X. Tao and J. Yang, *J. Chem. Sci.*, 2015, **127**, 375–382.

35 A. Helal and H. S. Kim, *Tetrahedron Lett.*, 2009, **50**, 5510–5515.

36 O. David, S. Maisonneuve and J. Xie, *Tetrahedron Lett.*, 2007, **48**, 6527–6530.

37 S. Yin, J. Zhang, H. Feng, Z. Zhao, L. Xu, H. Qiu and B. Tang, *Dyes Pigm.*, 2012, **95**, 174–179.

38 S. Lee, J. H. Lee, T. Pradhan, S. L. Chang, B. R. Cho, S. Bhuniya, S. Kim and J. S. Kim, *Sens. Actuators, B*, 2011, **160**, 1489–1493.

39 S. A. El-Safty, M. Khairy and M. Ismael, *Sens. Actuators, B*, 2012, **166–167**, 253–263.

40 W. Li, Z. Nie, K. He, X. Xu, Y. Li, Y. Huang and S. Yao, *Chem. Commun.*, 2011, **47**, 4412–4414.

41 Z. Xu, G.-H. Kim, S. J. Han, M. J. Jou, C. Lee, I. Shin and J. Yoon, *Tetrahedron*, 2009, **65**, 2307–2312.

42 S. Lee, Y.-S. Nam, Ho-J. Lee, Y. Lee and K.-B. Lee, *Sens. Actuators, B*, 2016, **237**, 643–651.

43 Z. Li, M. Yu, L. Zhang, *et al.*, *Chem. Commun.*, 2010, **46**, 7169–7171.

44 A. E. Lee, M. R. Grace, A. G. Meyer and K. L. Tuck, *Tetrahedron Lett.*, 2010, **51**, 1161–1165.

45 M. Li, H. Lu, R. Liu, J. Chen and C. Chen, *J. Org. Chem.*, 2012, **77**, 3670–3673.

46 Y. Ding, Y. Xie, X. Li, J. P. Hill, W. Zhang and W. Zhu, *Chem. Commun.*, 2011, **47**, 5431–5433.

47 (*a*) A. Ghorai, J. Mondal and G. K. Patra, *New J. Chem.*, 2016, **40**, 7821–7830; (*b*) A. K. Manna, J. Mondal, K. Rout and G. K. Patra, *J. Photochem. Photobiol., A*, 2018, **367**, 74.

48 (*a*) K. Rout, A. K. Manna, M. Sahu and G. K. Patra, *Inorg. Chim. Acta*, 2019, **486**, 733–741; (*b*) G. K. Patra, R. Chandra,

A. Ghorai and K. K. Shrivas, *Inorg. Chim. Acta*, 2017, **462**, 315–322.

49 *SMART & SAINT Software Reference manuals, version 5.0*, Bruker AXS Inc., Madison, WI, 1998.

50 T. Gruene, H. W. Hahn, A. V. Luebben, F. Meilleur and G. M. Sheldrick, *J. Appl. Crystallogr.*, 2014, **47**, 462.

51 (*a*) L. J. Farrugia, *WinGX: An Integrated System of Windows Programs for the Solution, Refinement and Analysis for Single Crystal X-ray Diffraction Data, version 1.80.01*, Department of Chemistry: University of Glasgow, 2003; (*b*) L. J. Farrugia, WinGX suite for small-molecule single-crystal crystallography, *J. Appl. Crystallogr.*, 1999, **32**, 837.

52 S. Ganguli, M. K. Panigrahi, P. Singh and P. K. Shukla, One-pot synthesis of novel quinazoline derivatives and their antimicrobial activity, *Int. J. Pharm. Pharm. Sci.*, 2012, **4**, 434.

53 A. K. Manna, S. Chowdhury and G. K. Patra, *Dalton Trans.*, 2019, **48**, 12336–12348.

54 M. J. Frisch, G. W. Trucks, H. B. Schlegel, G. E. Scuseria, M. A. Robb, J. R. Cheeseman, G. Scalmani, V. Barone, B. Mennucci, G. A. Petersson, H. Nakatsuji, M. Caricato, X. Li, H. P. Hratchian, A. F. Izmaylov, J. Bloino, G. Zheng, J. L. Sonnenberg, M. Hada, M. Ehara, K. Toyota, R. Fukuda, J. Hasegawa, M. Ishida, T. Nakajima, Y. Honda, O. Kitao, H. Nakai, T. Vreven, J. A. Montgomery Jr, J. E. Peralta, F. Ogliaro, M. Bearpark, J. J. Heyd, E. Brothers, K. N. Kudin, V. N. Staroverov, R. Kobayashi, J. Normand, K. Raghavachari, A. Rendell, J. C. Burant, S. S. Iyengar, J. Tomasi, M. Cossi, N. Rega, J. M. Millam, M. Klene, J. E. Knox, J. B. Cross, V. Bakken, C. Adamo, J. Jaramillo, R. Gomperts, R. E. Stratmann, O. Yazyev, A. J. Austin, R. Cammi, C. Pomelli, J. W. Ochterski, R. L. Martin, K. Morokuma, V. G. Zakrzewski, G. A. Voth, P. Salvador, J. J. Dannenberg, S. Dapprich, A. D. Daniels, Ö. Farkas, J. B. Foresman, J. V. Ortiz, J. Cioslowski and D. J. Fox, *Gaussian 09, Revision C.01*, GaussianInc., Wallingford, CT, 2009.

55 (*a*) A. D. Becke, *J. Chem. Phys.*, 1993, **98**, 5648; (*b*) C. Lee, W. Yang and R. G. Parr, *Phys. Rev. B: Condens. Matter Mater. Phys.*, 1988, **37**, 785.

56 M. K. Goshisht, G. K. Patra and N. Tripathi, *Mater. Adv.*, 2022, **3**, 2612.

57 V. K. Gupta, A. K. Singh, L. K. Kumawat and N. Mergu, *Sens. Actuators, B*, 2016, **222**, 468.

58 Y. Wang, C. Xi, Z. Han, Y. Jiao, X. Yao, Z. Lun, S. Fu, H. Zhang, P. Hou and D. Ning, *J. Photochem. Photobiol., B*, 2019, **199**, 111602.

59 J. H. Kang and C. Kim, *Photochem. Photobiol. Sci.*, 2018, **17**, 442.

60 C. A. S. Pothulapadu, A. Jayaraj, N. Swathi, R. N. Priyanka and G. Sivaraman, *ACS Omega*, 2021, **6**, 24473.

61 V. Kumar, D. Singh, P. Kumar, G. Chaudhary, A. P. Singh and R. Gupta, *J. Mol. Struct.*, 2022, **1261**, 132901.